



Published in final edited form as:

*Brain Stimul.* 2022 ; 15(6): 1552–1564. doi:10.1016/j.brs.2022.12.003.

## Differential dose responses of transcranial focused ultrasound at brain regions indicate causal interactions

Pai-Feng Yang<sup>a,b</sup>, M. Anthony Phipps<sup>a</sup>, Allen T. Newton<sup>a,b</sup>, Sumeeth Jonathan<sup>a,c</sup>, Thomas J. Manuel<sup>a,c</sup>, John C. Gore<sup>a,b,c</sup>, William A. Grissom<sup>a,c</sup>, Charles F. Caskey<sup>a,b</sup>, Li Min Chen<sup>a,b,\*</sup>

<sup>a</sup>Vanderbilt University Institute of Imaging Science, Vanderbilt University, Nashville, TN, USA

<sup>b</sup>Department of Radiology and Radiological Sciences, Vanderbilt University Medical Center, Nashville, TN, USA

<sup>c</sup>Department of Biomedical Engineering, Vanderbilt University, Nashville, TN, USA

### Abstract

We have previously shown that focused ultrasound (FUS) pulses in low pressure range exerted bidirectional and brain state-dependent neuromodulation in the nonhuman primate somatosensory cortices by fMRI. Here we aim to gain insights about the proposed neuron selective modulation of FUS and probe feedforward versus feedback interactions by simultaneously quantifying the stimulus (FUS pressures: 925, 425, 250 kPa) and response (% BOLD fMRI changes) function at the targeted area 3a/3b and off-target cortical areas at 7T. In resting-state, lowered intensities of FUS resulted in decreased fMRI signal changes at the target area 3a/3b and off-target area 1/2, S2, MCC, insula and auditory cortex, and no signal difference in thalamic VPL and MD nuclei. In activated states, concurrent high-intensity FUS significantly enhanced touch-evoked signals in area 1/2. Medium- and low-intensity FUS significantly suppressed touch-evoked BOLD signals in all areas except in the auditory cortex, VPL and MD thalamic nuclei. Distinct state dependent and dose-response curves led us to hypothesize that FUS's neuromodulatory effects may be mediated through preferential activation of different populations of neurons. Area 3a/3b may have distinct causal feedforward and feedback interactions with Area 1/2, S2, MCC, insula, and VPL. FUS offers a noninvasive neural stimulation tool for dissecting brain circuits and probing causal functional connections.

This is an open access article under the CC BY-NC-ND license (<http://creativecommons.org/licenses/by-nc-nd/4.0/>).

\*Corresponding author. Department of Radiology and Radiological Sciences, Institute of Imaging Science, Vanderbilt University Medical Center, AA 1105 MCN, 1161 21st Ave. S., Nashville, TN, 37232, USA. limin.chen@vanderbilt.edu (L.M. Chen).

CRedit contribution statement

**Pai-Feng Yang:** Methodology, Investigation, Visualization, Writing – original draft. **M. Anthony Phipps:** Methodology, Investigation, Visualization, Writing – review & editing. **Allen T. Newton:** Methodology, Investigation. **Sumeeth Jonathan:** Methodology, Investigation. **Thomas J. Manuel:** Visualization, Writing – review & editing. **John C. Gore:** Writing – review & editing. **William A. Grissom:** Methodology, Investigation, Writing – review & editing. **Charles F. Caskey:** Conceptualization, Methodology, Investigation, Supervision, Writing – review & editing. **Li Min Chen:** Conceptualization, Methodology, Investigation, Supervision, Writing – review & editing, Writing – original draft.

Declaration of competing interest

The authors declare no competing interests.

## Keywords

Transcranial focused ultrasound; Primates; fMRI; Neuromodulation; Brain circuit; Hand; Somatosensory

---

## 1. Introduction

Regions and circuits within a healthy brain interact in a coordinated fashion to maintain and execute various functions, while dysfunction in specific networks underlies many psychiatric and neurological disorders [1-3]. Targeted neuromodulation of a particular brain region by focused ultrasound (FUS) has emerged as a powerful tool for evaluating the contributions of individual brain regions to specific operations and functions in both healthy and disease conditions [4-8]. Transcranial FUS has strong therapeutic potential for rebalancing network activities because of its non-invasiveness and high spatial resolution. MRI-guided FUS (MRgFUS) allows precision targeting with real-time feedback and simultaneous functional monitoring. These capacities are essential for evaluating the effects and consequences of neuromodulation and reporting actions of FUS at both target and network levels.

Previous FUS studies have used varying parameters in different experimental models and reported both excitation and suppression effects on the target, but the precise mechanisms of action of FUS on neurons remain elusive [5]. The outcomes of FUS modulation at a particular intensity are net results of activated large excitatory pyramidal and small inhibitory interneurons. The ability to simultaneously monitor FUS actions at both target and off-target regions offers an effective way to examine the neural basis of FUS effects because the activity of only excitatory neurons can propagate beyond the local brain region and lead to detectable BOLD (blood oxygenation level dependent) signal changes at downstream off-target brain regions [9]. Using BOLD fMRI as a functional readout, we previously demonstrated that 250 kHz US pulses at 925 kPa free-field pressure (which we designate 'high' FUS pressure for this study) can excite local neurons in targeted somatosensory areas 3a/3b as well as downstream, inter-connected neurons in off-target brain regions [9]. Moreover, medium-intensity FUS (425 kPa) modulated neural activity in both positive (excitation) and negative (inhibitory) directions in a manner dependent on the brain state (resting or activation). These observations led us to propose that 250 kHz FUS of varying intensities may preferentially modulate populations of neurons to result in net excitation or inhibition of neural activity at the target and alter network function. A full appreciation of these modulatory effects requires a better understanding of the state-dependent dose-response function that relates FUS conditions to changes in neural activity.

This study aims to quantify the dose-response curve by delivering FUS pulses to target somatosensory areas 3a/3b in the macaque brain at three pressures: (i) high amplitude - 925 kPa (high-FUS), medium amplitude - 425 kPa (med-FUS), and low amplitude - 200 kPa (low-FUS). Note that even though we used terms of high, medium, and low amplitudes for description purpose, all three FUS intensities are in the low-intensity range, compared to high-intensity FUS used in ablation procedures. We also monitored FUS off-target influence on functions of other tactile regions and circuits. We employed our recently developed

MR-ARFI and robust fMRI paradigms that allow us to accurately localize the FUS beam and perform reliable mapping of touch networks in the brains of macaque monkeys [10-15]. Here we report that graded decreases of FUS intensities resulted in distinct dose-response curves in resting and activation states at the target. Off-target modulation effects also differed markedly as a function of FUS intensity. These observations of state-dependence provide additional insights to build into our hypothesis that 250 kHz FUS pulses may exert neuron-population-selective modulation in an intensity-dependent manner. Adding selective capabilities to FUS neuromodulation to promote suppression or enhancement based on neuron population state along with FUS parameters would add an additional layer of neurological tunability to FUS therapies and increase clinical impact.

## 2. Materials and methods

### 2.1. Animal preparation

Two female adult macaque monkeys (*M. fascicularis*) underwent six MRI experiments (three for each monkey). A total of 38 runs of fMRI scans were collected. Animals were initially sedated with ketamine hydrochloride (10 mg/kg), pre-medicated with atropine sulfate (0.05 mg/kg), and then anesthetized with isoflurane (1.0–1.5%) delivered in oxygen via mechanical ventilation. The head of each animal was placed in a custom-designed MR stereotaxic frame for stabilization during scans. The head was immobilized during the experiments with a set of ear bars, eye bars, and bite bar. Fig. 1A shows the schematic experimental scan setup. During functional MRI data acquisition, animals were maintained at a light (0.85–1.0% isoflurane) and stable level of anesthesia. A solution of 2.5% dextrose in saline was infused intravenously (10 ml/kg/h) to prevent dehydration. The temperature was maintained by means of a circulating water blanket. Heart rate and peripheral capillary oxygen saturation (SpO<sub>2</sub>; Nonin), respiration pattern and end-tidal CO<sub>2</sub> (24–32 mmHg; SurgiVet) were continuously monitored and maintained during the entire procedure. Animals were monitored closely for three days after each scan was completed. All procedures were conducted in accordance with National Institutes of Health guidelines and were approved by the Institutional Animal Care and Use Committee of Vanderbilt University.

### 2.2. Stimulation presentation paradigm

The fingers were stabilized with modeling clay, palm side up, leaving the glabrous skin of the distal finger pads available for stimulation (Fig. 1B). During fMRI data acquisition, innocuous tactile stimuli were delivered by vertical indentation (0.44 mm vertical displacement) of two rounded probes (diameter = 2 mm) at 8 Hz on the distal finger pads of D2 and D3 of the left hand. Probes were attached to piezoelectric actuators driven by an S88 Grass stimulator. Tactile stimulation was presented in 30-sec on and 30-sec off blocks. The probes-maintained contact with the skin of the digits during baseline periods.

FUS pulses were delivered in a block-based scheme identical to the tactile stimuli. During an “on” block, a 250 kHz, 300 ms pulse was emitted with a 3-s intersonication interval from a spherically focused MR-compatible transducer (diameter = 64 mm ROC = 63.2 mm, H115 Sonic Concepts, Bothell, WA) coupled via a custom water cone filled with 80% D<sub>2</sub>O (Deuterium oxide, or heavy water) that had been undisturbed for 24 h to allow large

bubbles to float out of the solution. The D<sub>2</sub>O was used to replace most of the H<sub>2</sub>O to reduce signal intensities and geometric distortions of MR images due to the ineffective shimming associated with the presence of high intensity H<sub>2</sub>O signals outside the brain. A single 300 ms pulse consisted of 63-cycle bursts repeated at 2 kHz (50% duty cycle). See Fig. 1C for FUS pulse design. The FUS transducer was driven by an arbitrary waveform generator (Agilent 33511B, Santa Clara, CA, USA) connected to an RF power amplifier (E&I A150, Rochester, NY, USA). The free-field peak negative pressures (PNP) at the spatial focus during this pulse were 925 kPa, 425 kPa, and 200 kPa for high, medium, and low conditions, corresponding to un-derated mechanical indexes (MI) of 0.9, 1.3, and 1.9. Estimating the spatial peak pulse average (ISPPA) from a sinusoidal pulse in brain tissue (sound speed 1562 m/s and density of 1030 kg/m<sup>3</sup>) yields 1.24 W/cm<sup>2</sup>, 5.6 W/cm<sup>2</sup>, and 26.6 W/cm<sup>2</sup>, and spatial peak temporal average (ISPTA) of 62 mW/cm<sup>2</sup>, 280 mW/cm<sup>2</sup>, 1329 mW/cm<sup>2</sup>. When derated to 58% (based on hydrophone measurements through ex vivo skull as in Yang et al., 2018 [9]), these values are MI = 0.68, 1.0, and 1.46, ISPPA values of 0.4 W/cm<sup>2</sup>, 1.9 W/cm<sup>2</sup>, and 8.9 W/cm<sup>2</sup>, and ISPTA values of 20.9 mW/cm<sup>2</sup>, 94 mW/cm<sup>2</sup>, and 446 mW/cm<sup>2</sup>. The acoustic interactions outside of the head at the skull are complex, and the main risk is scalp or skull heating during these procedures. We measured the temperature rise in the brain and muscle outside the skull using phase images acquired during fMRI. The maximum temperature rise detected was 2°C in the high-pressure condition, while we measured < 0.5°C in the medium FUS condition, which matches our prior observations and thermal simulations [9].

A custom microcontroller program coordinated pulsing for tactile, FUS, and tactile + FUS stimulation. The procedure resulted in 10 FUS bursts per “on” block. The maximum free-field pressure of the transducer was measured by placing a calibrated needle (for spatial peak pressures at which the MI was less than 1.4, H-0400, Onda Corp.) or fiber optic hydrophone (at higher pressures, FOH, Precision Acoustics, Dorchester, UK) at the focus of the transducer and recording the peak negative pressure at different input amplitudes.

### 2.3. Use of optical tracking and MRI-ARFI mapping methods to localize ultrasound beam on target

Repeated FUS delivery to the target with high precision is critical for our studies. We first used optical tracking for stereotactic neuro-navigation and to guide the FUS beam to the targeted 3a/3b tactile areas that were pre-defined by fMRI. Five 15 mm MRI-visible fiducial markers (MM3002, IZI Medical Products, Owings Mills, MD) were placed on the stereotactic frame (one on each eye bar and three on the two ear bars) to enable optical tracking outside the MRI scanner. A T1-weighted image was acquired for fiducial localization and anatomical imaging. The NHP was then brought out of the scanner room and optical tracking was used to position the FUS transducer was positioned over area 3a/3b on the right hemisphere contralateral to the tactile stimulation of the left hand. Transmission gel was placed over the shaved scalp to ensure adequate acoustic coupling. The NHP head was fixed in place on a table which could be moved into and out of the scanner room. We would acquire a set of image guidance scans then bring the NHP out of the scanner room to perform optical tracking. The trackers themselves are MR compatible but the camera is not. After tracking, the transducer would be locked into place and the NHP brought back into the MR room. Details of our optical tracking based FUS targeting method followed our

prior work [16]. By employing the same procedures as these prior studies, we expect that our targeting registration error will be approximately 3 mm, which is within the reported full-width at half maximum pressure of the transducer focus (ellipsoidal 6 mm × 39 mm). However, with the skull in beam path and only having a single slice of MR-ARFI data, it is possible that this error could be larger.

Before fMRI scanning, we confirmed the location and actual delivery of FUS with transcranial MR-acoustic radiation force imaging (MR-ARFI) [17], which measures the transient tissue displacements (proportional to acoustic intensity) induced by a short FUS pulse to map the ultrasound beam *in situ* as described below. Displacement images were acquired using a 2D single-slice spin-echo MRI acquisition (12.0 × 12.0 cm<sup>2</sup> FOV; 60 × 60 matrix; 2.0 × 2.0 mm<sup>2</sup> voxel size; 1 slice; 4.0 mm slice thickness; TE/TR 17/1000 ms) with unipolar motion-encoding gradients (3 ms duration; 40 mT m<sup>-1</sup> strength) to generate ARFI contrast. The motion-encoding gradients were oriented parallel to the ultrasound beam and the image slice was prescribed at the optically tracked location of the acoustic focus. Sonications were performed at the third harmonic of the transducer (802 kHz) for 4.5 ms (3609 cycles) with a maximum free-field pressure of 2.81 MPa and a duty cycle of 0.23%. The higher pressure and frequency were needed to generate sufficient displacement to be detectable with our MR-ARFI sequence. Displacement images were reconstructed using complex phase subtraction of four phase images with switched polarity motion-encoding gradients and with or without sonications, which were acquired in an interleaved fashion, for a total scan time of 4.0 min to produce one displacement image. Images were reconstructed offline in MATLAB 2017a (MathWorks, Natick, MA). Our MR-ARFI beam mapping method was non-invasive and followed prior work of ours and others [17-20]. More details are available about the use of this transducer for MR-ARFI at the third harmonic, including estimates of thermal deposition and discussion of possible error, in a prior publication [17].

Partial volume ARFI images were later registered based on the header information in the file (ie. the transformation that places the slices in the imaging space) and fiducial markers. These were overlaid on high-resolution T2-weighted structural images and corresponding detected BOLD activation foci for target confirmation. There may be small shifts due to image acquisition parameters such as EPI imaging shifts. We have visually compared magnitude images of partial volumes acquired during ARFI to geometrically stable acquisitions performed at the same time. Qualitatively, the ARFI magnitude images were aligned within the size of the ARFI voxels. Detailed equations describing the coordinate transforms relating these image volumes (optically tracked FUS beam, MR-ARFI displacement image, and T2\*-weighted structural brain volume) are described in our prior work [16].

#### 2.4. MRI data acquisition

All MRI scans were performed on a 7T Philips Achieva magnet with a customized surface transmit-receive coil (inner diameter = 6 cm) centered over the post-central gyri of the right hemisphere where the primary (S1) and secondary (S2) somatosensory cortices reside. Three types of MR images were acquired. 3D T1-weighted high-resolution isotropic volume (THRIVE) images were obtained to localize the fiducial markers placed around the FUS

probe for aligning and localizing the FUS beam to structural MR images (TE = 1.89 ms, TR = 4 ms, 400 x 400 x 140 matrix, 0.35 x 0.35 x 2 mm<sup>3</sup> voxel size, flip angle 10°, NSA = 1). A series of nine T2\*-weighted multi-slice gradient echo high-resolution structural coronal images (TE = 27 ms, TR = 500 ms, 768 x 768 x 9 matrix, 0.104 x 0.104 x 1 mm<sup>3</sup> voxel size) were also collected. fMRI data were acquired from the same slices using a single-shot gradient-echo echo planar imaging (GE-EPI) sequence (TE = 16 ms, TR = 2 s, 0.625 x 0.625 x 1 mm<sup>3</sup> voxel size, 128 x 128 x 9 matrix, interleaved slices, linear k-space filling). fMRI data with tactile stimulation of digits and/or FUS were collected with the same fMRI acquisition parameters. In a typical fMRI session, a total of 2–4 runs were acquired. A total of 38 runs (two or three conditions for each run: Tactile and FUS or FUS + Tactile; Tactile, FUS and FUS + Tactile) from fourteen imaging sessions (high FUS: 11 runs, medium FUS: 16 runs, and low FUS: 11 runs) were included in the fMRI time course analysis.

## 2.5. fMRI data analysis

fMRI signals went through standard pre-processing steps of slice timing (3dTshift, AFNI) and 3-D motion correction (3dvolreg, AFNI), and were then spatially smoothed using an isotropic Gaussian filter kernel with a full width at half maximum of 1 mm (3dmerge, AFNI). Functional EPI images were up-sampled from 0.625 x 0.625 x 1 mm<sup>3</sup> to 0.312 x 0.312 x 1 mm<sup>3</sup>, and co-registered with corresponding T2\*-weighted high-resolution anatomical images using a linear image registration tool (3dAllineate, AFNI) for display. The fMRI BOLD EPI data were temporally smoothed with a low-pass filter with cutoff frequency of 0.25 Hz (fslmaths, FSL). BOLD data were analyzed in two steps: using general linear model analysis to generate activation maps during tactile stimulation and defining regions of interest (ROI) to extract BOLD time courses for calculating % BOLD signal changes.

fMRI activation maps were created by calculating the cross-correlation between the signal time courses of each voxel and the Hemodynamic Response Function (HRF) convolved stimulus presentation time course. We used a general linear model (3dDe-convolve, AFNI) approach to detect significant BOLD signal changes during the presentation of different stimulation conditions (FUS alone versus FUS + tactile). Our criteria for significant BOLD signal changes include (1) t values of 1.8–3.0 (equivalent of  $p = 0.05$  to 0.001) in a linear relation between BOLD time course and HRF predictor and (2) the minimal number of significant voxels within each cluster ( $n = 10$  EPI images voxels), and FDR ( $p < 0.05$ ) correction. Detected activation voxels were superimposed on the corresponding high-resolution T2\*-weighted anatomical images for display.

BOLD signals were extracted from voxels in the target (area 3a/3b) and seven off-target regions. Five of them including area 1/2, S2, Insula, MCC (Midcingulate cortex), and thalamus VPL (ventroposterior lateral) nucleus are known to be part of the tactile circuit and have shown consistent fMRI activations to tactile stimulation across scans and animals. Two off-network non-tactile regions (MD: mediodorsal nucleus and auditory cortex) were included as control ROIs. A macaque monkey brain atlas [21] was used to localize the stimulus-activated voxels to each ROI. ROI masks were manually defined according to the atlas. Raw BOLD signal time courses from voxels with a maximal  $t$ -value  $> 2.8$

within each ROI were extracted to quantify the amplitudes of the BOLD signal changes to stimulation. Percentage BOLD signal change was calculated by subtracting the mean baseline signal prior to stimulus onset from the mean BOLD signals of three peak volumes during the stimulation period, and then dividing it by the baseline signal (peak-baseline)/baseline. Baseline signal was calculated by averaging the signal amplitude of three image volumes before the stimulus onset. Time courses were fitted with a two-gamma function. The response peak for each condition and ROI was calculated by averaging raw BOLD signal amplitudes at three time points around the response peak identified by two-gamma fitting. Measures were then averaged across runs, scan sessions, and animals, and were examined for statistical significance using one-way ANOVA followed by Tukey's test between stimulation conditions. A  $p < 0.05$  was considered statistically significant. ROI-based BOLD time course plots are presented as the mean  $\pm$  standard error of the mean (SEM). Statistical analyses were performed using GraphPad Prism 9. Correlation analysis was performed between FUS intensity and peak BOLD signal curves between area 3a/3b and each off-target region.

### 3. Results

#### 3.1. FUS pulses activated neurons at the targeted area 3a/3b and off-target regions in resting versus tactile activation conditions

We have previously reported that high-intensity FUS elicited fMRI activation maps and medium-intensity FUS induced bidirectional modulation of brain activity [9,22]. Here we added fMRI activation maps detected during low-intensity FUS (low-FUS) stimulation (Fig. 2). Compared to tactile stimulation-evoked fMRI activation maps (Fig. 2A), delivery of low-intensity FUS at the target area 3a/3b elicited weak fMRI responses at the target and within the network (Fig. 2B). Concurrent presentation of tactile stimulation with low-FUS pulses suppressed the BOLD signals at the targeted area 3a/3b and led to a general reduction in the number of detected tactile activation foci at most off-target regions (Fig. 2C). To visualize the activation map differences between conditions, we plotted (tactile + FUS) - tactile (Fig. 2D) and (tactile + FUS) - FUS (Fig. 2E) subtraction maps. The blue patches indicate the stronger responses to tactile or FUS stimulation conditions. There are few overlaps between the blue patches in the two conditions. Our observations show that low FUS stimulation of area 3a/3b evoked activations in brain regions that are not part of the primary somatosensory network. We focused our ROI based time course analysis on those brain regions that responded to both FUS and tactile stimulation.

#### 3.2. Lower FUS intensities resulted in decreased BOLD responses at resting-state

We quantified the BOLD signal time courses by three FUS intensities at resting brain state (Fig. 3). Consistent with our previous observation, the BOLD signal change in the subcortical thalamus VPL nucleus (~0.2%) was weaker than those of cortical regions [9,22]. BOLD signals at the two off-circuit control regions (MD and auditory cortex) were very weak, fluctuating around the baseline except that in auditory cortex during high-FUS stimulation (Fig. 3B). Lower FUS pulse intensities elicited BOLD signal changes in a decreasing trend at the target area 3a/3b (high-medium-low: 0.46%, 0.25%, and 0.19%) and in varying degrees at off-target area 1/2 (0.46%, 0.29%, 0.15%), S2 (0.45%, 0.36%,

0.15%), MCC (0.35%, 0.34%, 0.18%), VPL (0.26%, 0.24%, 0.18%), MD (0.04%, 0.002%, 0.009%), auditory cortex (0.17%, 0.015%, 0.015%), and Insula (0.36%, 0.08%, 0.13%) (Fig. 3C). Among six ROIs, area 3a/3b, area 1/2, and insula exhibited peak BOLD signal changes elicited by high-FUS that were significantly larger than those elicited by med-FUS and low-FUS (Fig. 3C). S2 and MCC showed peak BOLD signal changes to low-FUS that were significantly lower than those elicited by high-FUS and med-FUS (Fig. 3C). Peak BOLD signal change in VPL did not differ significantly as a function of FUS intensity (last column group in Fig. 3C). In summary, the peak BOLD fMRI signal changes elicited by FUS stimulation at three intensities differed across on- and off-target regions.

### 3.3. Distinct suppressive effects of FUS intensities on tactile responses at different brain regions

We next examined the modulatory effects of concurrently delivering FUS pulses at three different intensities during tactile stimulation (Fig. 4). Compared to tactile stimulus evoked % BOLD signal changes, the simultaneous application of high-intensity FUS did not induce significant signal changes at the FUS-targeted area 3a/3b (tactile:  $0.48 \pm 0.05\%$ , high-FUS + tactile:  $0.45 \pm 0.05\%$ ) and six off-target regions (S2:  $0.46 \pm 0.04\%$ ,  $0.37 \pm 0.05\%$ ; insula:  $0.32 \pm 0.03\%$ ,  $0.34 \pm 0.04\%$ ; MCC:  $0.40 \pm 0.03\%$ ,  $0.40 \pm 0.04\%$ ; and VPL:  $0.23 \pm 0.03\%$ ,  $0.21 \pm 0.04\%$ ; MD:  $0.02\% \pm 0.01\%$ ,  $0.03 \pm 0.02\%$ ; and auditory cortex:  $0.11 \pm 0.02\%$ ,  $0.13 \pm 0.03\%$ ). However, at area 1/2 the BOLD signal was enhanced with concurrent high-FUS sonication ( $0.34 \pm 0.03\%$  to  $0.52 \pm 0.06\%$ , Fig. 4B & C). Med-FUS mostly suppressed the tactile responses at the targeted area 3a/3b (tactile:  $0.48 \pm 0.05\%$ , med-FUS + tactile:  $0.27 \pm 0.04\%$ ) and off-target insula ( $0.32 \pm 0.03\%$ ,  $0.19 \pm 0.05\%$ ), while low-FUS mostly suppressed the tactile responses at area 1/2 (tactile:  $0.34 \pm 0.03\%$ , low-FUS + tactile:  $0.23 \pm 0.03\%$ ), S2 ( $0.46 \pm 0.04\%$ ,  $0.26 \pm 0.04\%$ ), and MCC ( $0.40 \pm 0.03\%$ ,  $0.18 \pm 0.03\%$ , Fig. 4B & C). No suppression was observed in thalamic VPL. Percent signal change was a lower peak in control ROIs MD and auditory cortex, and signals were only about half that of VPL. In summary, both med-FUS and low-FUS suppressed tactile responses at the target. The same set of FUS intensities exerted differential modulatory effects at different off-target regions: enhancement (high-FUS area 1/2), suppression (S2, insula, and MCC), or no detectable change (VPL, MD, auditory cortex).

### 3.4. Distinct FUS dose-response relationships between the stimulated and interconnected regions via cortico-cortical and thalamic-cortical connections

Direct comparisons of dose-response curves at the stimulated target versus downstream or upstream interconnected off-target regions provide insights about the possible interactions between FUS pulses and neurons at the stimulation site and between stimulated and interconnected brain regions. Fig. 5A shows direct comparisons of FUS modulation of the resting (FUS alone, red) and activated (FUS + Tactile, green) brain states (three dots represent h (high), m (medium) or l (low) intensity FUS). Lowering FUS pulse intensity resulted in two distinct response curves at the targeted area 3a/3b (light orange shading in Fig. 5A and B): a graded decrease in BOLD signal change for resting state and a V-shaped trend in BOLD signal change during the tactile activation state (however, there is no statistical difference between med- and low-FUS). For the activation state, the medium intensity FUS induced the strongest suppression at the target (44% signal reduction) and

off-target insula (41%), while low-FUS mostly suppressed the tactile responses at area 1/2 (32%), S2 (44%), and MCC (54%, Fig. 5B). BOLD signal amplitudes in control MD and auditory cortex were weak and showed no apparent relations to FUS intensity (last two plots in Fig. 5A & B). When we used the area 3a/3b dose-response curves as references, we observed strong correlations ( $r > 0.6$ ) between the target area and all off-target regions in a resting state (Fig. 5C). However, in the activated state, the correlations between area 3a/3b and area 1/2, insula, and MCC remained high. The correlation between area 3a/3b and S2 was low ( $r = 0.17$ ), and the correlation between area 3a/3b and subcortical thalamus VPL ( $r = -0.56$ ) and MD ( $r = -0.98$ ) signal trends were negative (anti-correlated; Fig. 5D) in the activated state. In summary, all off-target cortical regions, except S2, followed the FUS dose-response curves at the FUS-targeted stimulation site (area 3a/3b) regardless of brain state. Dose-response curves between the stimulation site and the off-target subcortical thalamus VPL nucleus showed a reversed trend in the activated state. Dose-response curves in the outside network regions showed weak signal and distinct relative relationships. Fig. 5E revealed that tactile stimulation evoked responses were weaker in all off-target regions.

To evaluate whether there are differences in temporal signal to noise ratios (tSNR) of cortical versus subcortical regions, we computed tSNR in all eight regions on the right hemisphere where the surface coil and ultrasound transducer were targeted. TSNRs (mean  $\pm$  SEM) at subcortical regions (VPL =  $35 \pm 1.7$  and MD =  $36 \pm 1.7$ ) were slightly weaker than cortical regions (area 3a/3b =  $42 \pm 1.7$ , area 1/2 =  $42 \pm 1.5$ , S2 =  $38 \pm 1.4$ , insula =  $38 \pm 1.3$ , MCC =  $40 \pm 1.5$ , and auditory =  $39 \pm 1.3$ ). The mean tSNR difference is very small (2.33) between cortical (39.8) and subcortical (37.5) regions.

### 3.5. Modulation of the tactile network with varying FUS intensities

To appreciate the modulatory effects of FUS at the network level, we plotted the network response profile at all eight ROIs at three FUS intensities (high-FUS, med-FUS, and low-FUS) and in three brain states (tactile activation alone, resting state + FUS, and tactile activation state + FUS; Fig. 5). High-FUS stimulation at either resting or activation state elicited comparable BOLD signal changes at the targeted area 3a/3b, MCC, and insula, but significant signal enhancements in area 1/2 at the activation state (compare solid red line with dotted red and blue lines in Fig. 6A). Med-FUS stimulation evoked BOLD signal changes are comparable in all regions in resting versus activation states, except in insula where a slight signal increase was detected in insula (compare solid and dotted orange lines in Fig. 6B). Low-FUS stimulation induced the most apparent changes at the network level. All brain regions, except VPL and MCC, showed strong state-dependent BOLD signal changes (compare solid and dotted magenta lines in Fig. 6C). In summary, the strongest state-dependent network profile changes were detected in the low-FUS condition whereas the weakest changes were detected in the high-FUS condition.

### 3.6. Proposed theoretical model of neuron type-selective modulation of 250 kHz FUS

Fig. 7 illustrates a proposed neuron type selective modulation of high- versus medium- and low-FUS intensities at the targeted area 3a/3b and its direct influences on those off-target somatosensory regions that are interconnected via different feedback versus feedforward connections. Fig. 7A shows a simplified version of the known projecting and processing

pathways for tactile inputs originating from peripheral hand skin. During tactile stimulation of digits, ascending inputs arrive at VPL through the spinal cord, then project to the first cortical relay and integration station, area 3a/3b, and then to higher order areas 1/2, S2, Insula, and MCC. Both excitatory and inhibitory neurons are activated at each relay/processing station; however, the net responses are excitatory with the output signals carried by large projection excitatory pyramidal neurons at each station (ROIs in our case). Fig. 7B shows these parallel projecting pathways during direct FUS stimulation of resting area 3a/3b. At rest, varying intensities of FUS predominantly activated excitatory projecting neurons and thus led to robust BOLD signal changes at target area 3a/3b and interconnected cortical and subcortical regions. FUS-activated neurons at area 3a/3b send outgoing signals via cortico-cortical feedforward connections to cortical regions of area 1/2, S2, Insula, and MCC in decreasing strength, and via cortico-thalamic feedback connections to VPL in the thalamus. When area 3a/3b is directly activated by FUS, the direction of information flow to thalamus changed from feedforward afferents during tactile stimulation to feedback afferents during FUS stimulation.

Fig. 7C illustrates the proposed FUS neuron type selective neuromodulation model in the resting and tactile activated states. In the resting state, FUS pulses likely activate predominantly excitatory communicative pyramidal neurons at target area 3a/3b and subsequently lead to activations of neurons in the interconnected brain regions (left panel in Fig. 7C). In the activated state, concurrently delivered varying intensities of FUS pulses interact with neurons activated by tactile input and exert different modulatory effects likely by activating both large excitatory pyramidal neurons and small inhibitory interneurons in different proportions. Activity of neurons at each off-target region reflects the net outcomes of the interaction between outputs from area 3a/3b (by FUS) and incoming tactile inputs (by digit stimulation). Because high-FUS did not induce any suppressive effects, we propose that high-FUS predominately activated a larger proportion of excitatory neurons relative to inhibitory interneurons (middle panel in Fig. 7C). In contrast, we propose that med-FUS and low-FUS pulses activated a larger proportion of inhibitory interneurons relative to excitatory neurons because these FUS intensities markedly suppressed tactile activations (right panel in Fig. 7C). A higher proportion of activated inhibitory neurons would result in reduction in tactile response magnitude and lead to weaker output signals in area 1/2, MCC, S2, and Insula. Because subcortical VPL and MD nuclei exhibited no modulation effects by varying FUS intensities, we speculate that the strength of the cortico-cortical or cortico-thalamic connections between area 3a/3b and each off-target ROI and the direction (feedforward versus feedback) of the underlying anatomical connections likely contributed to the distinct modulation effects.

#### 4. Discussion

We and others have previously demonstrated that FUS with varying parameters in the 220–250 kHz pulse frequency range can lead to both excitatory and inhibitory neural modulation, but with limited knowledge about dose responses and mechanisms of actions on neurons and networks [23-25]. By monitoring the effects of FUS modulation with fMRI, we previously observed bidirectional and state-dependent FUS modulation of fMRI signals at the target and off-target regions when blocks of 250 kHz FUS pulses at 925

kPa (classified as high-intensity FUS) and 425 kPa (classified as medium-intensity FUS) intensities were delivered at the primary somatosensory cortex area 3a/3b in resting and tactile activation states [9,22]. These prior observations led us to hypothesize that FUS pulses presented at different intensities may selectively modulate activity of excitatory and inhibitory neurons in a state-dependent manner. This study tested this hypothesis by quantifying the dose-response function at target area 3a/3b and examining its relationship to dose responses of off-target cortical and subcortical regions that are known to have extensive and differential feedforward and feedback anatomical and functional connections to area 3a/3b. We observed distinct FUS dose-fMRI response curves at the target during rest versus activation states. The dose-response curves at off-target regions varied depending on the degrees of feedforward versus feedback connections; therefore, the curves can be used to probe causal functional relationships between brain regions.

#### 4.1. Dose responses of FUS at the stimulated versus remote interconnected regions

We chose three FUS intensities (high-FUS: 925 kPa, med-FUS: 425 kPa, and low-FUS: 220 kPa) for dose-response quantification. These intensities were selected based on our own simulation and prior theoretical modeling work which suggests that 250 kHz FUS pulses with these amplitudes likely induce excitatory and/or inhibitory modulatory effects [26,27]. Our previous observations with high-FUS and med-FUS, which were replicated in the current study, further support the hypothesis that med-FUS results in intensity-dependent, bidirectional neuromodulation. Two features of the FUS dose – fMRI response curves observed are novel and of interest: (i) distinct relationships in resting versus activated states at the target and (ii) different curves at off-target cortical versus subcortical regions. For example, the fMRI signal changes at the target area reflected the interactions between FUS pulses and all neurons that reside in that cortical location, including both large excitatory projection neurons and local small inhibitory interneurons. Increasing the intensity of FUS pulses evoked linearly increasing fMRI BOLD signals in a resting state (Fig. 3). This linear relationship suggests that FUS in the intensity range tested directly and proportionally excited resting neurons. In theory both inter-area projection neurons and local interneurons could be modulated. Because only projection pyramidal neurons send communicative output signals to interconnected brain regions, linear activation of pyramidal neurons at the target should lead to graded linear activation of downstream neurons at off-target regions. Indeed, FUS pulses of three intensities activated interconnected neurons in remote regions within the same functional network (the touch network in our case) and beyond (Fig. 2) [9], likely via propagating spiking activity. Others have reported similar observations in the visual and somatosensory systems of humans and non-human primates [28-33]. Interestingly, we observed similar linear BOLD signal increases in cortical areas 1/2, S2, and MCC (Figs. 4 and 5). This linear response curve supports the excitatory effects of FUS pulses in the resting cortex. Both interconnected cortical and subcortical regions followed the dose-response curve of the stimulation site (Fig. 6C).

Because area 3a/3b is the first cortical relay station for tactile processing, we speculate that the dose-response curve relationships between this cortical target and its interconnected cortical areas 1/2, S2, insula, and MCC could be attributed to their distinct feedforward connections. Area 1/2, S2, insula, and MCC are considered downstream higher order cortical

regions to area 3a/3b and receive strong feedforward inputs from area 3a/3b [34-37]. In contrast, the thalamus VPL nucleus is an upstream input feeding region to area 3a/3b. Neural activity elicited by FUS at the area 3a/3b travels to VPL via feedback connections, which are much weaker than the feedforward connections. The second possibility for the varying modulation effects across ROIs could be that the strength of connections and the volume of neurons at the output receiving region (off-target) varied. Dose-response curves observed in the control out of somatosensory network regions of MD and auditory cortex further support the role of inter-regions connectivity. Nevertheless, because only activated projection neurons can drive off-target activation, dose-response analysis at the off-target region provides insights about the properties of the output excitation signal that originated from the stimulation site (target).

#### 4.2. The brain state-dependence of FUS modulation

Neuronal activity differs in resting versus activation states and different types of neurons are engaged. In our study, we induced neural activation by peripheral tactile stimulation of the skin of the hand. Concurrent delivery of FUS at linearly decreasing intensities at the activated cortex, which is involved in the processing of peripheral tactile inputs, allows us to compare the dose-response differences in resting versus activation state. We found that graded decreases of FUS intensity concomitant with tactile stimulation resulted in nonlinear BOLD signal changes at the target, compared to the linear decreasing BOLD signals in cortex in the absence of stimulation. Off-target neural responses to FUS stimulation varied in amplitude and locations. At the target, the strongest BOLD signal drop, compared to the tactile and high-FUS responses occurred during the med-FUS stimulation condition (Fig. 5). Suppression of tactile responses could result from reduced activity of pyramidal neurons or enhanced activity of inhibitory interneurons. Area 3a/3b is the first cortical relay station for innocuous tactile inputs, so these BOLD signal reductions could also be direct consequences of reduced driven activity from area 3a/3b by med-FUS. The detected BOLD signal could be a net outcome of these two possible processes. Because the linearly changing FUS intensities were kept identical during both resting or tactile activation states, the linear versus nonlinear FUS dose - BOLD response curve further supports our speculation that FUS interaction with neurons could be neuron-type specific, depending on the FUS intensity and brain states. Medium-intensity FUS likely activated a larger proportion of inhibitory neurons, which subsequently suppressed the fMRI responses to tactile stimulation. There have been similar observations reported in different studies; however, here we reported them within the same experimental preparation. The application of such FUS pulses to rats [38] and rabbits [39] resulted in a reduction of somatosensory evoked potentials [40]. FUS with parameters in a similar range also inhibited the amplitude of single transcranial magnetic stimulation (TMS) pulse elicited motor evoked potentials in human motor cortex [41].

Our study revealed complex and interrelated interactions within and across different brain regions. These state-dependent (activation versus rest) dual modulatory effects at the target led us to speculate that activation (stimulation) and suppression effects of med-amplitude FUS could be mediated through stimulating different populations of neurons (i.e., excitatory pyramidal neurons and small inhibitory interneurons). The physiological state (active or rest) of neurons in the stimulated region and its circuit and how these neurons interact

with each other during modulation could also influence the net outcome. For example, pyramidal cells in cortical layer IV of areas 3a/3b receive predominantly cutaneous tactile and proprioceptive inputs from the thalamic VPL nucleus. These pyramidal cells process information via local microcircuits and then send outputs to higher order areas 1/2 and S2 by pyramidal cells at deeper layer V. Large pyramidal cells are also surrounded by local small interneurons that are predominantly inhibitory. During local processing and integration, small interneurons interact with pyramidal neurons, modulate their activity, and sometimes gate their output information [42]. Direct activation of pyramidal neurons by FUS could subsequently excite interconnected neurons in different off-target regions via propagated spiking activity. It is possible that the connection strength and/or the number of synaptic connections play a role in differing downstream neural modulations. Nevertheless, these findings are significant because they indicate that FUS may act differently on different populations of neurons, based on network and FUS properties. FUS has potential to probe direct causal functional relationships between brain regions and to dissect brain circuits with some level of neuron-selectivity [43].

#### 4.3. Modulating different neuron types by varying FUS intensity

The scientific basis for hypothesizing that FUS pulses show cell-type selectivity is that diverse expression of mechanosensitive ion channels across neurons underlies differential responses to ultrasound. We speculate that FUS pulses presented at different intensities likely preferentially modulated one type of neuron over another. For example, at the cellular level, neocortex is composed of two main types of neurons – large glutamatergic excitatory neurons (predominantly pyramidal neurons) and small GABAergic inhibitory interneurons [44]. Projection pyramidal neurons send outputs to downstream brain regions while local interneurons participate in local information integration and can modulate the excitability of pyramidal neurons [45]. The distributions of mechanosensitive ion channels likely vary across these two types of neurons, which could lead to differential reactions to external FUS pulses. In addition to the neuron size and number differences, the ion channel and membrane excitation status of these two types of neurons also differs significantly during resting versus activation states. In our case, activation state means both neurons and interneurons are activated and engaged in the processing of tactile inputs originating from the peripheral hand skin. High intensity FUS stimulation of area 3a/3b elicited comparable BOLD signal changes, suggesting that FUS likely activated pyramidal and interneurons in similar ways as tactile stimulation of hand. The action of FUS pulses on neurons at rest that require little energy compared to active state neurons that are experiencing dynamic transmembrane ion flows could differ markedly. Thus, under such drastically different circumstances, the modulatory effects of FUS at the target likely reflect the net outcome of FUS's interaction with different types of neurons in different states at the target area. Support for this speculation comes from our calcium imaging study of mouse sensorimotor cortex brain slices where we found that FUS pulses with similar frequency could activate excitatory pyramidal neurons [46]. Additionally, others have shown that activity of regular spiking units (presumed to be excitatory neurons) in the rat sensory cortex increases with increasing pulse repetition frequency, while fast-spiking units (presumed to be inhibitory neurons) were not responsive to FUS [43]. In addition to the key features of neuron size and distribution of mechanoreceptive ion channels on each type of neuron that may underlie the state-dependent

modulation of FUS, other factors such as the neuron swelling during activation and cell compositional features may also have contributed. For instance, when neurons are activated (i.e., due to engagement in information processing), influx of ions could lead to neuron body swelling [47-49]. Such change in neuron body shape could alter the distribution or sensitivity of FUS wave sensing mechanoreceptive ion channels.

#### **4.4. Complex functional relationship between FUS stimulated and downstream brain regions: implications for interpreting neuromodulation results**

The brain is an inter-connected system and perturbation of any node in the system would alter functions of the target node and those of interconnected downstream brain regions. We think that functional consequences of FUS neuromodulation at the target and its functional networks are reflective of local interactions between FUS waves and neuron activity at the target and are influenced by the degree of reciprocal connections between target and off-target areas. It is known that neuron type compositions and properties vary across cortical and subcortical areas and across species [50]. The possibility of neuron-type selective modulation of FUS is of high clinical significance since it likely will influence the efficacy of using FUS modulation as a therapeutic intervention. The net FUS modulatory effects will not only be determined by the FUS parameters but also by the activation state of the brain, which could be drastically different in patients. The current study provided the first characterization of dose-response characteristics in the nonhuman primate brain. The dose-response curves likely differ across cortical and subcortical regions, and distinct neuron type compositions across cortical and subcortical regions likely contribute to these differences.

There are three potential issues that need to be considered in the interpretation of our results. First is the slow temporal nature of fMRI signals. The sluggish signal prevents testing feedforward and feedback information flow. The second issue relates to the fact that BOLD fMRI signals are indirect neuronal activity indices and reflective of energy demands of both excitatory and inhibitory neurons [51,52]. Suppression of excitatory and inhibitory neurons can lead to reduced BOLD signal changes; however, the output signals to the downstream regions would differ if modulation were neuron-type selective. Direct neuronal electrophysiology recordings and neuron type manipulations can tease out differential modulatory effects of FUS on excitatory versus inhibitory neurons [43]. Potentially, some of the BOLD responses we detected in the target region reflected the effects of FUS on the vasculature or the activity of glial cells rather than neurons. While analysis of dose-response curves at off-target regions allows assessment of spiking-based inter-area communications, direct spiking and local field potential recordings would be needed to parcellate the neuron-type specific modulations in vivo. Nevertheless, we have shown previously in the same system that BOLD signal changes are tightly associated with spiking and local field potential activities [10,53,54]. The third issue relates to the effects of anesthesia employed in the current study. We have extensively studied these brain regions under the same light isoflurane anesthesia with intracranial electrophysiology and found good correlations between BOLD fMRI and electrophysiology local field potential (LFP) signals in both activation and resting states [53,55,56]. These previous observations led us to speculate that the anesthesia may have a similar effect on FUS induced BOLD

signal changes, such that increased anesthesia would reduce the overall strengths of the FUS induced neural modulation and BOLD signal magnitudes. Our focus has been on quantifying the FUS dose dependent BOLD signal response curves, without testing effects of anesthesia levels directly. We expect an evenly distributed reduction with increasing anesthesia across different FUS doses, therefore, anesthesia level would not alter the overall trend of the dose-response curve. Nevertheless, the influences of anesthesia on BOLD signals at rest require future investigation.

The last issue relates to FUS's potential skull and scalp heating and associated brain responses. It is possible that when the transducer is turned on, it could create a sensation in the scalp, which could result in fMRI activation in the somatosensory cortex in the regions of the face/head representation. However, we think the possibility is low for two main reasons. Firstly, the temperature increases are small. The main perceivable interactions that could occur are the acoustic radiation force and temperature rise. The acoustic radiation force can be perceived at regions known to be sensitive to force (e.g., fingers as in Ref. [57]), although the estimated radiation force in our study is much lower. The temperature increases were smaller. We extracted phase information from a subset of the high pressure fMRI studies and estimated the temperature rise in the brain and in muscle immediately outside of the skull based on MR thermometry. In the brain, the maximum temperature rise detected in the high-pressure group was approximately  $0.5^{\circ}C$ ; which is comparable to thermal simulations from our prior work [Yang et al., 2018]. Among high-pressure cases, the maximum observed temperature increase in the muscle was approximately  $2^{\circ}C$ . Because heat deposition is proportional to intensity (ie. square of pressure), we expect that the low and medium cases will have significantly lower thermal rise.

Secondly, we think that the possibility of scalp activation being attributed to S2 cortex is low. Based on the somatosensory topographic organization of the body, the representations of hand regions and the skull skin on the cortex are separated in space. In our case, if sensation were evoked by the FUS or FUS-induced temperature increase, it would be represented predominantly in the cortical areas (e.g., area 3b/area 1 or S2) on the opposite hemisphere of the FUS stimulation site (contralateral to tactile stimulated hand). Additionally, in the present study, we used hand stimulation evoked fMRI activation foci as guidance to place the FUS target. We thus have the confidence that we only stimulated the hand cortex region. Our careful examination of the ARFI pressure field indeed showed quite spatially constrained FUS beam target and path. The negligible BOLD signals detected in thalamic MD and auditory cortex (except high FUS), which are located near VPL, S2, and insula, indicate that FUS induced BOLD activations at off-target regions are not spill-over effects. We think that coactivation of scalp under FUS transducer would not confound the observed FUS-intensity dependent responses at the hand cortical representation region in area 3a/3b.

Lastly, our experimental design minimized their interferences in quantifying the FUS dose and BOLD response functions. For example, we have two built-in controls within the two stimulation conditions: FUS alone versus tactile + FUS. These two experimental conditions share the same features of ultrasound stimulation of skull skin. With such a design, the shared inputs from the skull skin were identical and subtracted out. Additionally, taken

together, it is unlikely that such a small temperature increase at the scalp can lead to widespread brain activations that would confound the observed FUS-intensity dependent responses at the cortical hand representation region in area 3a/3b.

There is another possibility that the smaller neuromodulation effects of FUS in thalamic VPL and MD regions are due to their deep brain locations and a worse signal-to-noise ratio (tSNR). However, our tSNR measurements from all eight ROIs showed that there were no systematic tSNR differences between cortical versus subcortical regions. We believe that the distinct FUS modulation of cortical versus subcortical VPL regions is a result of modulation via feedback versus feedforward connections.

A major hurdle in circuit mapping and manipulation is the precision of the tool that can locally activate or inactivate the chosen brain target. In our case, FUS beam was targeted at area 3a/3b and evoked BOLD activation at the target and off-target regions. We do not think the activation in off-target regions were a direct result of FUS due to their close location to the path of the ultrasound. We have simulated and mapped the FUS pressure field carefully. The ARFI maps showed that the FUS path was quite constrained. While the separation of area 3a/3b and area 1/2 may not be as clear, the spatial distances were within the range of separation between area 3a/3b and other cortical areas.

#### 4.5. Effects of FUS on the auditory cortex

Auditory cortex activation may be attributed to both mechanical and neuronal mechanisms. Activation in the auditory cortex has been reported under FUS stimulation [58,59]. Different mechanisms have been proposed. Bone conduction has been proposed as a means for the vibration to be connected to the cochlea [60]. However, it has also been shown that elimination of the auditory pathway does not preclude FUS stimulation from occurring [61] as well as work in cultured neurons and brain slices [39,46]. In this study there are at least two sources of auditory frequencies in the detectable range for non-human primates (<40 kHz) [62]: the 2 kHz PRF within each sonication and the repeated square wave envelopes, which generates a wide range of frequencies. Similar sonication patterns have been reported to produce a detectable auditory effect in human studies [63]. In this study the presence of the fMRI sequence may act as a partial mask, but the ear bars used in the frame will likely reduce the environmental noise level while the FUS induced bone conduction noise will still be present.

Our observation of differential FUS-induced BOLD response curves between auditory and cortex and the target during high FUS intensity condition, med-FUS and low-FUS conditions, supports a neural origin. If the auditory cortex activation were attributed entirely to bone conduction, we would expect very similar dose response curves at the target area 3a/3b and auditory cortex; however, the FUS dose response curves in the auditory cortex did not increase with increased FUS intensity (shown in Fig. 3). Comparison of dose response curves at target and off-target regions allow us to separate mechanical versus neuronal contributions. Thus, we attribute FUS-associated auditory cortex activation at least partially to possible direct functional connections between somatosensory cortex to auditory cortex. Interactions between the auditory and somatosensory cortices have been well-documented. For example, event-related potentials recorded from scalp electrodes in human subjects in

response to paired auditory and somatosensory stimulus conditions resulted in multisensory event-related potentials at earlier times (50 ms) post-stimulus compared to single modality stimulation [64]. Other studies show multisensory interactions occurring early in processing in low-level sensory cortical areas [65,66]. Together, our results support a neural origin of auditory activation during FUS, rather than being the result of only an auditory effect.

In conclusion, we observed state-dependent dual excitatory and inhibitory effects on target neurons and evaluated causal effects of activated area 3a/3b on activities of downstream higher order cortical areas 1/2, S2, MCC, insula, and upstream thalamic VPL nucleus. The distinct dose-response curves in resting versus activated states and at stimulated versus off-target regions support the neuron-selective modulation of 250 kHz FUS in the 220-925k Pa intensity range. 250 kHz FUS may exert a spectrum of neuromodulatory effects likely via selective activation of varying proportions of excitatory and/or inhibitory neurons and depends on the state of the brain. The dose-response curves at off-target somatosensory regions revealed their distinct and state-dependent hierarchical functional organization.

## Acknowledgments

We would also like to acknowledge expert assistance from Chaohui Tang for animal handling support and Drs. Jamie Reed and Jordan Racca for language editing of the manuscript draft.

## Funding

National Institutes of Health, United States: R01MH111877 (CFC, LMC), R24MH109105 (CFC, LMC), 1S10OD012297-01A1(JCG), 5T32EB014841(JCG), and 1F31EB026928 (SJ).

## Abbreviations:

<b>FUS</b>	focused ultrasound
<b>fMRI</b>	functional magnetic resonance imaging
<b>BOLD</b>	blood-oxygenation-level-dependent imaging
<b>MR-ARFI</b>	magnetic resonance-acoustic radiation force imaging
<b>HRF</b>	hemodynamic response function
<b>ROI</b>	region of interest
<b>area 3a/3b</b>	primary somatosensory cortex area 3a and area 3b
<b>VPL</b>	ventroposterior lateral nucleus
<b>S2</b>	secondary somatosensory cortex
<b>Ins</b>	insular cortex
<b>MCC</b>	Midcingulate cortex
<b>MD</b>	mediodorsal nucleus

## References

- [1]. Assaf M, Jagannathan K, Calhoun VD, Miller L, Stevens MC, Sahl R, et al. Abnormal functional connectivity of default mode sub-networks in autism spectrum disorder patients. *Neuroimage* 2010;53(1):247–56. [PubMed: 20621638]
- [2]. Fingelkurts AA, Kahkonen S. Functional connectivity in the brain—is it an elusive concept? *Neurosci Biobehav Rev* 2005;28(8):827–36. [PubMed: 15642624]
- [3]. Fox MD, Halko MA, Eldaief MC, Pascual-Leone A. Measuring and manipulating brain connectivity with resting state functional connectivity magnetic resonance imaging (fcMRI) and transcranial magnetic stimulation (TMS). *Neuroimage* 2012;62(4):2232–43. [PubMed: 22465297]
- [4]. Naor O, Krupa S, Shoham S. Ultrasonic neuromodulation. *J Neural Eng* 2016;13(3):031003. [PubMed: 27153566]
- [5]. Blackmore J, Shrivastava S, Sallet J, Butler CR, Cleveland RO. Ultrasound neuromodulation: a review of results, mechanisms and safety. *Ultrasound Med Biol* 2019;45(7):1509–36. [PubMed: 31109842]
- [6]. Kamimura HAS, Conti A, Toschi N, Konofagou EE. Ultrasound neuromodulation: mechanisms and the potential of multimodal stimulation for neuronal function assessment. *Front Physiol* 2020;8.
- [7]. Darmani G, Bergmann TO, Butts Pauly K, Caskey CF, de Lecea L, Fomenko A, et al. Non-invasive transcranial ultrasound stimulation for neuromodulation. *Clin Neurophysiol* 2022;135:51–73. [PubMed: 35033772]
- [8]. Zhang T, Pan N, Wang Y, Liu C, Hu S. Transcranial focused ultrasound neuromodulation: a review of the excitatory and inhibitory effects on brain activity in human and animals. *Front Hum Neurosci* 2021;15:749162. [PubMed: 34650419]
- [9]. Yang PF, Phipps MA, Newton AT, Chaplin V, Gore JC, Caskey CF, et al. Neuromodulation of sensory networks in monkey brain by focused ultrasound with MRI guidance and detection. *Sci Rep* 2018;8(1):7993. [PubMed: 29789605]
- [10]. Chen LM. Cortical representation of pain and touch: evidence from combined functional neuroimaging and electrophysiology in non-human primates. *Neurosci Bull* 2018;34(1):165–77. [PubMed: 28466257]
- [11]. Chen LM, Dillenburg BC, Wang F, Friedman RM, Avison MJ. High-resolution functional magnetic resonance imaging mapping of noxious heat and tactile activations along the central sulcus in New World monkeys. *Pain* 2011;152(3):522–32. [PubMed: 21177033]
- [12]. Chen LM, Turner GH, Friedman RM, Zhang N, Gore JC, Roe AW, et al. High-resolution maps of real and illusory tactile activation in primary somatosensory cortex in individual monkeys with functional magnetic resonance imaging and optical imaging. *J Neurosci* 2007;27(34):9181–91. [PubMed: 17715354]
- [13]. Chen LM, Yang PF, Wang F, Mishra A, Shi Z, Wu R, et al. Biophysical and neural basis of resting state functional connectivity: evidence from non-human primates. *Magn Reson Imaging* 2017;39:71–81. [PubMed: 28161319]
- [14]. Wu R, Wang F, Yang PF, Chen LM. High-resolution functional MRI identified distinct global intrinsic functional networks of nociceptive posterior insula and S2 regions in squirrel monkey brain. *Neuroimage* 2017;155:147–58. [PubMed: 28461059]
- [15]. Wu R, Yang PF, Chen LM. Correlated disruption of resting-state fMRI, LFP, and spike connectivity between area 3b and S2 following spinal cord injury in monkeys. *J Neurosci* 2017;37(46):11192–203. [PubMed: 29038239]
- [16]. Chaplin V, Phipps MA, Jonathan SV, Grissom WA, Yang PF, Chen LM, et al. On the accuracy of optically tracked transducers for image-guided transcranial ultrasound. *Int J Comput Assist Radiol Surg* 2019;14(8):1317–27. [PubMed: 31069643]
- [17]. Phipps MA, Jonathan SV, Yang PF, Chaplin V, Chen LM, Grissom WA, et al. Considerations for ultrasound exposure during transcranial MR acoustic radiation force imaging. *Sci Rep* 2019;9(1):16235. [PubMed: 31700021]

- [18]. Hertzberg Y, Volovick A, Zur Y, Medan Y, Vitek S, Navon G. Ultrasound focusing using magnetic resonance acoustic radiation force imaging: application to ultrasound transcranial therapy. *Med Phys* 2010;37(6):2934–42. [PubMed: 20632605]
- [19]. Gaur P, Casey KM, Kubanek J, Li N, Mohammadjavadi M, Saenz Y, et al. Histologic safety of transcranial focused ultrasound neuromodulation and magnetic resonance acoustic radiation force imaging in rhesus macaques and sheep. *Brain Stimul* 2020;13(3):804–14. [PubMed: 32289711]
- [20]. Ozenne V, Constans C, Bour P, Santin MD, Valabregue R, Ahnine H, et al. MRI monitoring of temperature and displacement for transcranial focus ultrasound applications. *Neuroimage* 2020;204:116236. [PubMed: 31597085]
- [21]. Saleem KS, Logothetis NK. A combined MRI and histology atlas of the rhesus monkey brain in stereotaxic coordinates. second ed. Elsevier/Academic Press; 2012.
- [22]. Yang PF, Phipps MA, Jonathan S, Newton AT, Byun N, Gore JC, et al. Bidirectional and state-dependent modulation of brain activity by transcranial focused ultrasound in non-human primates. *Brain Stimul* 2021;14(2):261–72. [PubMed: 33460838]
- [23]. Deffieux T, Younan Y, Wattiez N, Tanter M, Pouget P, Aubry JF. Low-intensity focused ultrasound modulates monkey visuomotor behavior. *Curr Biol* 2013;23(23):2430–3. [PubMed: 24239121]
- [24]. Wattiez N, Constans C, Deffieux T, Daye PM, Tanter M, Aubry JF, et al. Transcranial ultrasonic stimulation modulates single-neuron discharge in macaques performing an antisaccade task. *Brain Stimul* 2017;10(6):1024–31. [PubMed: 28789857]
- [25]. Fomenko A, Neudorfer C, Dallapiazza RF, Kalia SK, Lozano AM. Low-intensity ultrasound neuromodulation: an overview of mechanisms and emerging human applications. *Brain Stimul* 2018;11(6):1209–17. [PubMed: 30166265]
- [26]. Plaksin M, Kimmel E, Shoham S. Cell-type-selective effects of intramembrane cavitation as a unifying theoretical framework for ultrasonic neuromodulation. *eNeuro* 2016;3(3). ENEURO.0136-15.2016.
- [27]. Fomenko A, Chen KS, Nankoo JF, Saravanamuttu J, Wang Y, El-Baba M, et al. Systematic examination of low-intensity ultrasound parameters on human motor cortex excitability and behavior. *Elife* 2020;9.
- [28]. Lee W, Kim H, Jung Y, Song I-U, Chung YA, Yoo S-S. Image-guided transcranial focused ultrasound stimulates human primary somatosensory cortex. *Sci Rep* 2015;5.
- [29]. Lee W, Kim HC, Jung Y, Chung YA, Song IU, Lee JH, et al. Transcranial focused ultrasound stimulation of human primary visual cortex. *Sci Rep* 2016;6:34026. [PubMed: 27658372]
- [30]. Folloni D, Verhagen L, Mars RB, Fouragnan E, Constans C, Aubry JF, et al. Manipulation of subcortical and deep cortical activity in the primate brain using transcranial focused ultrasound stimulation. *Neuron* 2019;101(6):1109–16. [PubMed: 30765166]
- [31]. Verhagen L, Gallea C, Folloni D, Constans C, Jensen DE, Ahnine H, et al. Offline impact of transcranial focused ultrasound on cortical activation in primates. *Elife* 2019;8:e40541. [PubMed: 30747105]
- [32]. Legon W, Sato TF, Opitz A, Mueller J, Barbour A, Williams A, et al. Transcranial focused ultrasound modulates the activity of primary somatosensory cortex in humans. *Nat Neurosci* 2014;17(2):322–9. [PubMed: 24413698]
- [33]. Ai L, Bansal P, Mueller JK, Legon W. Effects of transcranial focused ultrasound on human primary motor cortex using 7T fMRI: a pilot study. *BMC Neurosci* 2018;19(1):56. [PubMed: 30217150]
- [34]. Cerkevich CM, Kaas JH. Corticocortical projections to area 1 in squirrel monkeys (*Saimiri sciureus*). *Eur J Neurosci* 2019;49(8):1024–40. [PubMed: 29495078]
- [35]. Kaas JH. Evolution of somatosensory and motor cortex in primates. *Anat Rec A Discov Mol Cell Evol Biol* 2004;281(1):1148–56. [PubMed: 15470673]
- [36]. Wu CW, Bichot NP, Kaas JH. Converging evidence from microstimulation, architecture, and connections for multiple motor areas in the frontal and cingulate cortex of prosimian primates. *J Comp Neurol* 2000;423(1):140–77. [PubMed: 10861543]
- [37]. Evrard HC. The organization of the primate insular cortex. *Front Neuroanat* 2019;13:43. [PubMed: 31133822]

- [38]. Kim H, Park MY, Lee SD, Lee W, Chiu A, Yoo SS. Suppression of EEG visual-evoked potentials in rats through neuromodulatory focused ultrasound. *Neuroreport* 2015;26(4):211–5. [PubMed: 25646585]
- [39]. Yoo SS, Bystritsky A, Lee JH, Zhang Y, Fischer K, Min BK, et al. Focused ultrasound modulates region-specific brain activity. *Neuroimage* 2011;56(3):1267–75. [PubMed: 21354315]
- [40]. Dallapiazza RF, Timbie KF, Holmberg S, Gatesman J, Lopes MB, Price RJ, et al. Noninvasive neuromodulation and thalamic mapping with low-intensity focused ultrasound. *J Neurosurg* 2018;128(3):875–84. [PubMed: 28430035]
- [41]. Legon W, Bansal P, Tyshynsky R, Ai L, Mueller JK. Transcranial focused ultrasound neuromodulation of the human primary motor cortex. *Sci Rep* 2018;8(1):10007. [PubMed: 29968768]
- [42]. Chu J, Anderson SA. Development of cortical interneurons. *Neuropsychopharmacology* 2015;40(1):16–23. [PubMed: 25103177]
- [43]. Yu K, Niu X, Krook-Magnuson E, He B. Intrinsic functional neuron-type selectivity of transcranial focused ultrasound neuromodulation. *Nat Commun* 2021;12(1):2519. [PubMed: 33947867]
- [44]. Parnavelas JG. The origin and migration of cortical neurones: new vistas. *Trends Neurosci* 2000;23(3):126–31. [PubMed: 10675917]
- [45]. Kapfer C, Glickfeld LL, Atallah BV, Scanziani M. Supralinear increase of recurrent inhibition during sparse activity in the somatosensory cortex. *Nat Neurosci* 2007;10(6):743–53. [PubMed: 17515899]
- [46]. Manuel TJ, Kusunose J, Zhan X, Lv X, Kang E, Yang A, et al. Ultrasound neuromodulation depends on pulse repetition frequency and can modulate inhibitory effects of TTX. *Sci Rep* 2020;10(1):15347. [PubMed: 32948791]
- [47]. Cohen LB, Keynes RD, Hille B. Light scattering and birefringence changes during nerve activity. *Nature* 1968;218(5140):438–41. [PubMed: 5649693]
- [48]. Andrew RD, MacVicar BA. Imaging cell volume changes and neuronal excitation in the hippocampal slice. *Neuroscience* 1994;62(2):371–83. [PubMed: 7830884]
- [49]. Tasaki I Rapid structural changes in nerve fibers and cells associated with their excitation processes. *Jpn J Physiol* 1999;49(2):125–38. [PubMed: 10393347]
- [50]. Gilman JP, Medalla M, Luebke JI. Area-specific features of pyramidal neurons—a comparative study in mouse and rhesus monkey. *Cerebr Cortex* 2017;27(3):2078–94.
- [51]. Logothetis NK. The neural basis of the blood-oxygen-level-dependent functional magnetic resonance imaging signal. *Philos Trans R Soc Lond B Biol Sci* 2002;357(1424):1003–37. [PubMed: 12217171]
- [52]. Logothetis NK. What we can do and what we cannot do with fMRI. *Nature* 2008;453(7197):869–78. [PubMed: 18548064]
- [53]. Wang Z, Chen LM, Negyessy L, Friedman RM, Mishra A, Gore JC, et al. The relationship of anatomical and functional connectivity to resting-state connectivity in primate somatosensory cortex. *Neuron* 2013;78(6):1116–26. [PubMed: 23791200]
- [54]. Chen LM, Gore JC. 4.16 - mesoscale microcircuits within and across primate somatosensory areas identified with functional MRI. In: Fritzsche B, editor. *The senses: a comprehensive reference*. second ed. Oxford: Elsevier; 2020. p. 279–87.
- [55]. Pan WJ, Thompson G, Magnuson M, Majeed W, Jaeger D, Keilholz S. Broadband local field potentials correlate with spontaneous fluctuations in functional magnetic resonance imaging signals in the rat somatosensory cortex under isoflurane anesthesia. *Brain Connect* 2011;1(2):119–31. [PubMed: 22433008]
- [56]. Wang L, Saalman YB, Pinski MA, Arcaro MJ, Kastner S. Electrophysiological low-frequency coherence and cross-frequency coupling contribute to BOLD connectivity. *Neuron* 2012;76(5):1010–20. [PubMed: 23217748]
- [57]. Dalecki D, Child SZ, Raeman CH, Carstensen EL. Tactile perception of ultrasound. *J Acoust Soc Am* 1995;97(5 Pt 1):3165–70. [PubMed: 7759656]

- [58]. Guo H, Hamilton M 2nd, Offutt SJ, Gloeckner CD, Li T, Kim Y, et al. Ultrasound produces extensive brain activation via a cochlear pathway. *Neuron* 2018;98(5):1020–10230 e4. [PubMed: 29804919]
- [59]. Sato T, Shapiro MG, Tsao DY. Ultrasonic neuromodulation causes widespread cortical activation via an indirect auditory mechanism. *Neuron* 2018;98(5):1031–10341 e5. [PubMed: 29804920]
- [60]. Salahshoor H, Shapiro MG, Ortiz M. Transcranial focused ultrasound generates skull-conducted shear waves: computational model and implications for neuromodulation. *Appl Phys Lett* 2020;117(3):033702. [PubMed: 32741976]
- [61]. Mohammadjavadi M, Ye PP, Xia A, Brown J, Popelka G, Pauly KB. Elimination of peripheral auditory pathway activation does not affect motor responses from ultrasound neuromodulation. *Brain Stimul* 2019;12(4):901–10. [PubMed: 30880027]
- [62]. Coleman MN. What do primates hear? A meta-analysis of all known nonhuman primate behavioral audiograms. *Int J Primatol* 2009;30(1):55–91.
- [63]. Johnstone A, Nandi T, Martin E, Bestmann S, Stagg C, Treeby B. A range of pulses commonly used for human transcranial ultrasound stimulation are clearly audible. *Brain Stimul* 2021;14(5):1353–5. [PubMed: 34481096]
- [64]. Murray MM, Molholm S, Michel CM, Heslenfeld DJ, Ritter W, Javitt DC, et al. Grabbing your ear: rapid auditory-somatosensory multisensory interactions in low-level sensory cortices are not constrained by stimulus alignment. *Cerebr Cortex* 2005;15(7):963–74.
- [65]. Meredith MA, Lomber SG. Species-dependent role of crossmodal connectivity among the primary sensory cortices. *Hear Res* 2017;343:83–91. [PubMed: 27292113]
- [66]. Zhou YD, Fuster JM. Somatosensory cell response to an auditory cue in a haptic memory task. *Behav Brain Res* 2004;153(2):573–8. [PubMed: 15265656]

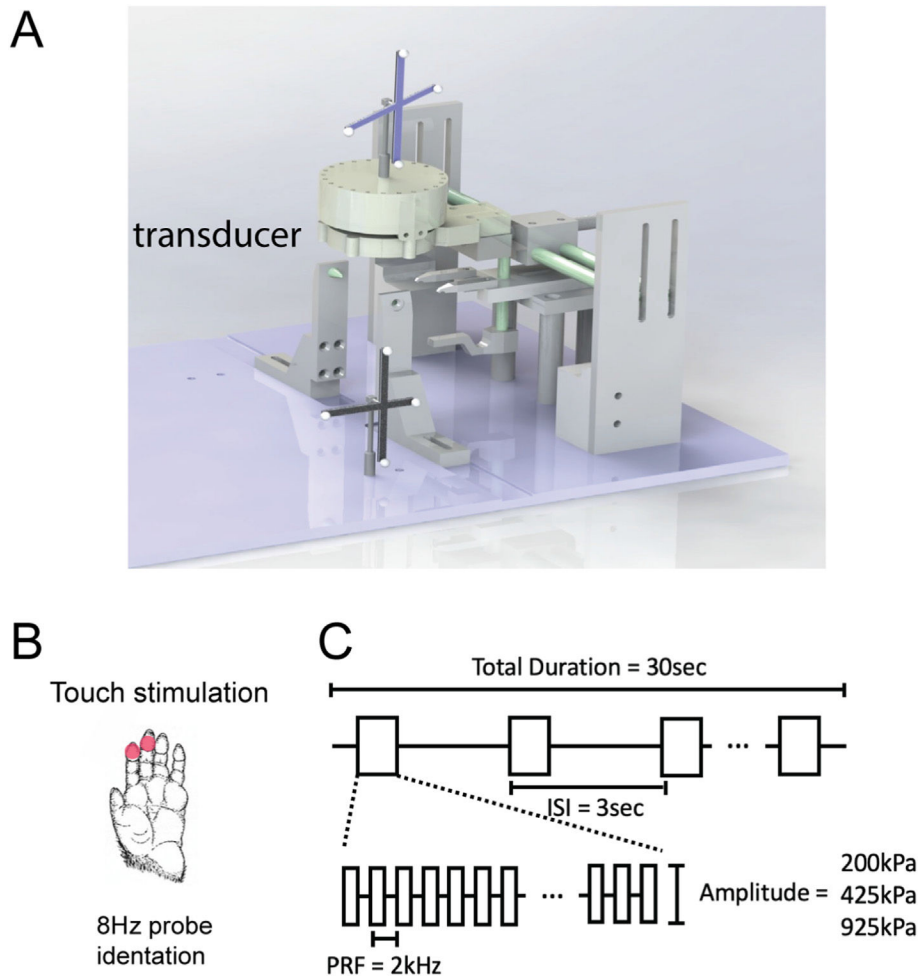


**Fig. 1. MRgFUS neuromodulation experimental setup.**

(A) A single FUS transducer was placed over the somatosensory area (3a/3b) hand region. (B) locations of tactile stimulation. (C) FUS pulse parameters. Three intensities of FUS pluses were delivered: 200 kPa (low), 425 kPa (medium), and 925 kPa (high). Ultrasound stimulation blocks were 30 s total with an inter-stimulation interval (ISI) of 3 s and a burst length of 300 ms. Each burst consisted of a 2 kHz pulse repetition frequency with a 250 us sonication for a 50% duty cycle.

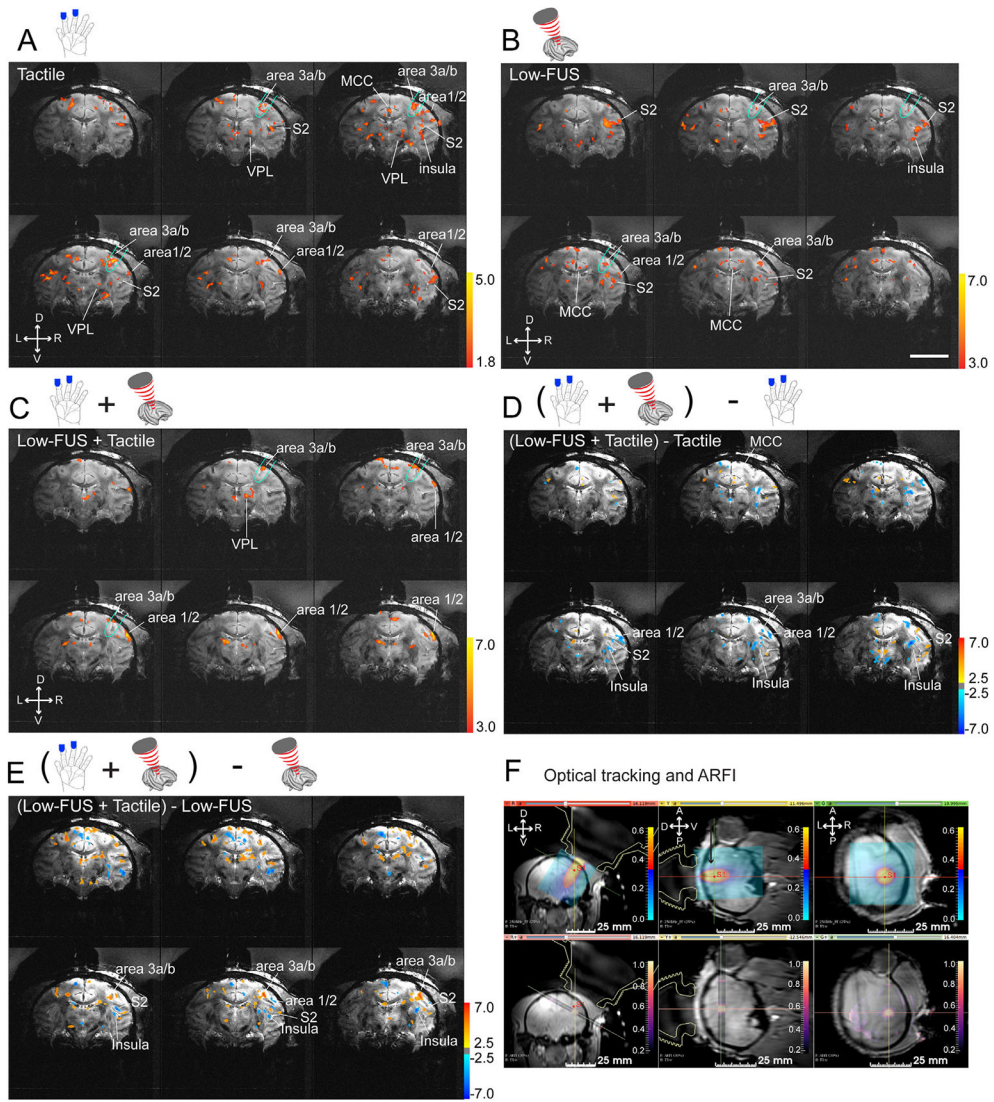


**Fig. 2. Concurrent sonication of areas 3a/3b with low-amplitude FUS pulses suppresses tactile stimulus-evoked fMRI BOLD activations in the brain of a macaque monkey.** (A) Multi-run coronal fMRI activation maps evoked by 8 Hz vibrotactile stimulation of the distal finger pads of digits 2 & 3 of the left hand. Activation maps are shown with thresholds  $t > 1.8$ ,  $p = 0.01$ ,  $q = 0.003$ , FDR ( $p < 0.05$ ) corrected. Six coronal images are arranged from caudal to rostral direction (top left to bottom right). Aqua outlines indicate the FUS beam location. (B–C) Multi-run coronal fMRI activation maps evoked by low amplitude FUS alone (B) or with concurrent delivery of tactile stimulation (C) of the areas 3a/3b region of the right hemisphere. Activation maps are shown with thresholds  $t > 3.0$ ,  $p = 0.001$ ,  $q = 0.003$ , FDR ( $p < 0.05$ ) corrected. (D) fMRI subtraction maps of tactile stimulation plus low amplitude FUS minus tactile stimulation. (E) fMRI subtraction maps of tactile stimulation plus low amplitude FUS minus low amplitude FUS. (F) Coronal (left), sagittal (middle) and oblique (right – perpendicular to the FUS beam) T1w images show optical tracking (top row) and MR-ARFI maps (bottom row, color scale bar: tissue displacement in mm) fMRI subtraction maps of tactile stimulation plus medium amplitude FUS minus tactile

stimulation. VPL: thalamic ventro-posterior lateral nucleus. Scale bar: 20 mm. D: dorsal. V: ventral. L: left. R: right. A: anterior. P: posterior.

Author Manuscript

Author Manuscript

Author Manuscript

Author Manuscript

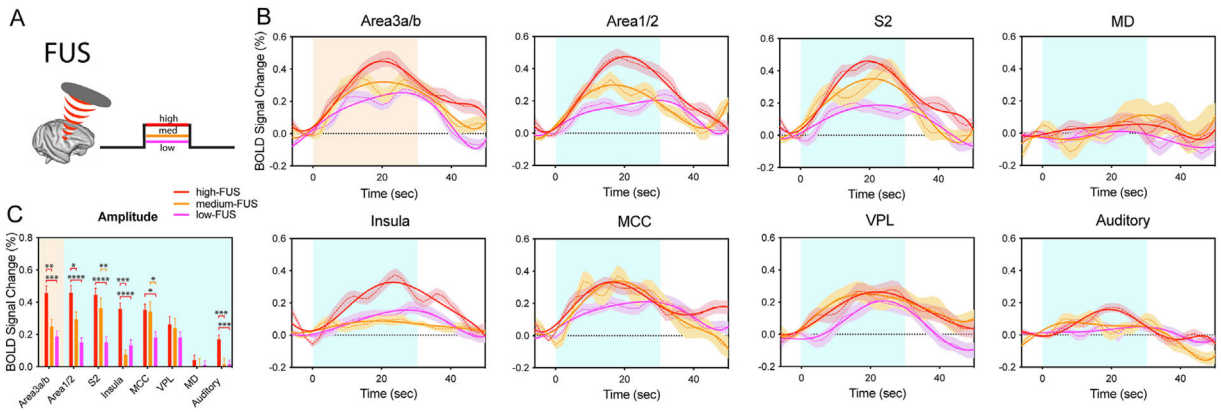


**Fig. 3. FUS intensity-dependent BOLD fMRI signal changes at the target and off-target regions.** (A) schematic illustration of the interleaved FUS and tactile stimulus presentation paradigm. Only one FUS intensity was presented in each fMRI run. (B) Dotted lines: mean time courses of % BOLD signal changes at the FUS-targeted area 3a/3b, and five off-target regions: area 1/2, secondary somatosensory cortex (S2), Insular cortex (insula), middle cingulate cortex (MCC), auditory cortex, and thalamic VPL and MD nuclei. Color shadow indicates  $\pm$  standard error of the mean. Solid lines: two gamma fitting curves of raw time course. Light orange and blue backgrounds indicate the 30-second duration of stimulation. (C) Bar plots of peak BOLD signal changes during tactile and FUS stimulation at three intensities shown for the target and off-target ROIs. \*  $p < 0.05$ , \*\*  $p < 0.01$ , \*\*\*  $p < 0.001$ , \*\*\*\*  $p < 0.0001$ , where the analysis was comprised of a one-way ANOVA test followed by Tukey's test for FUS intensity.

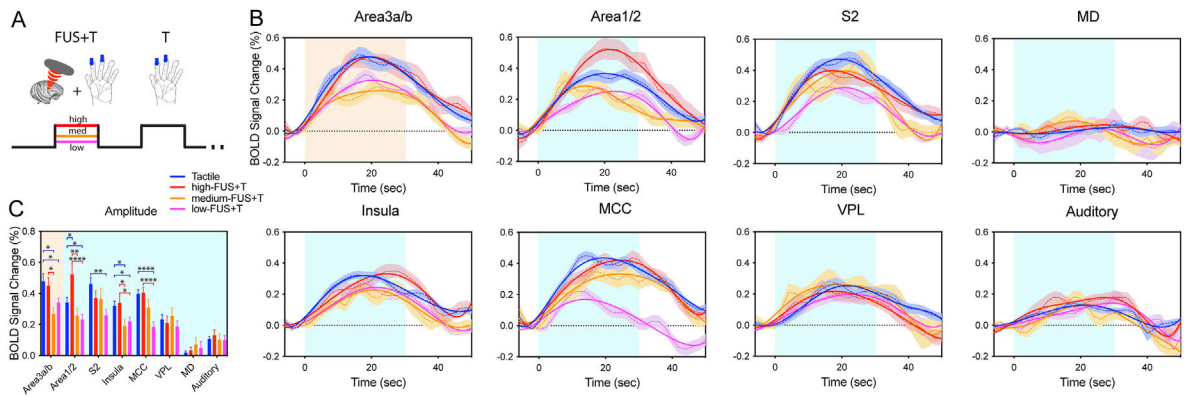


**Fig. 4. FUS intensity-dependent suppression of tactile stimulation-evoked BOLD fMRI signal changes at the target and off-target regions.**

(A) Schematic illustration of the interleaved simultaneous FUS + tactile and tactile stimulus presentation paradigm. Only one FUS intensity was presented in each fMRI run. (B) Time courses of % BOLD signal changes at the FUS target area 3a/3b, and five off-target regions of area 1/2, S2, insula, MCC, auditory cortex, and thalamus VPL and MD nuclei. Light orange and blue backgrounds indicate the 30 s duration of stimulation. (C) Bar plots of peak BOLD signal changes during tactile and FUS stimulation at three intensities shown for the target (light orange section) and off-target ROIs (light blue section). \* $p < 0.05$ , \*\* $p < 0.01$ , \*\*\* $p < 0.001$ , \*\*\*\* $p < 0.0001$ , where the analysis comprised a one-way ANOVA test followed by Tukey's test.

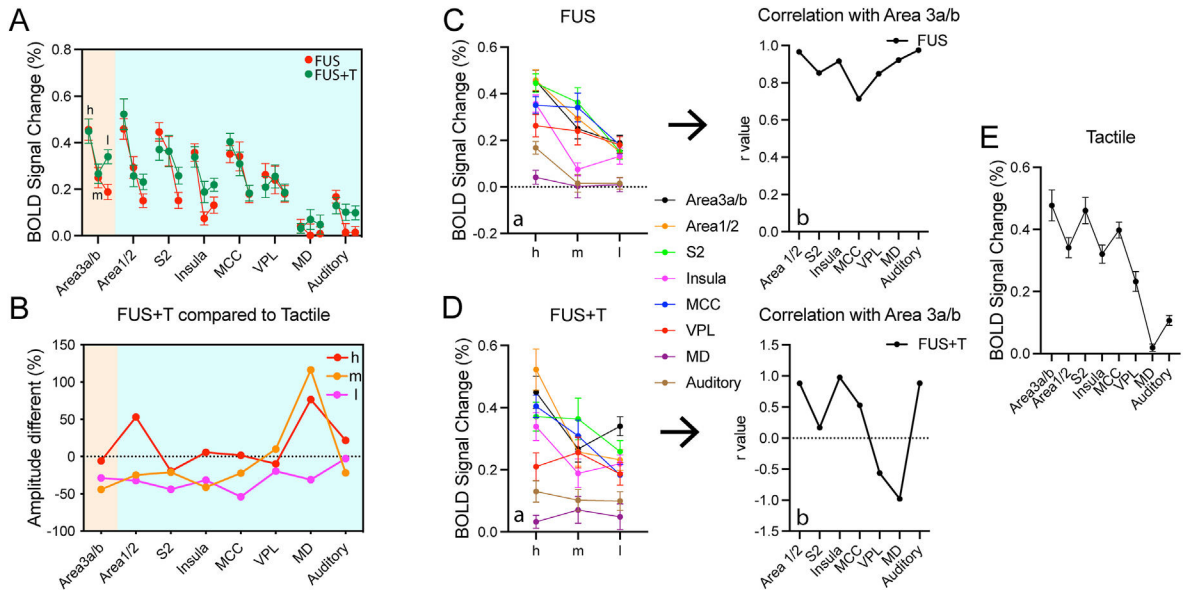


**Fig. 5. Correlation of FUS dose – fMRI responses between target and off-target regions in resting and activation states.**

(A) Plots of peak BOLD signal changes at the FUS-targeted area 3a/3b and seven off-target regions in response to FUS stimulation at three FUS intensities (h: high, m: medium, l: low) during FUS alone (red curves) and simultaneous FUS + Tactile (green curves) stimulation. (B) Plots of % BOLD signal differences between simultaneous FUS + tactile and tactile stimulation conditions (set as 100%) at each region. (C-D) Ca & Da: plots of BOLD signal changes at three FUS intensities across all regions at rest (Ca, FUS-alone condition) and activation (Da, FUS + tactile condition) states. Cb & Db: plots of correlation (r values) between area 3a/3b and each of the off-target regions. E: plots of % BOLD signal changes across all regions in response to tactile stimulation at left hand digits.

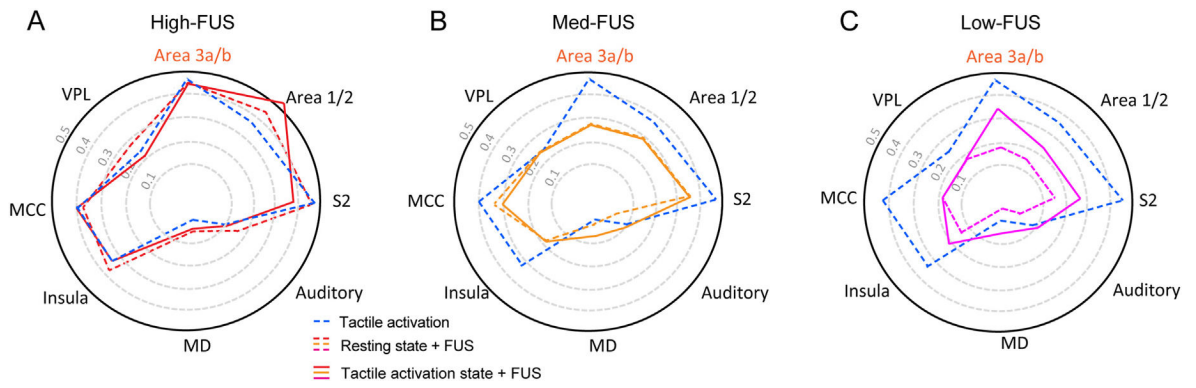


**Fig. 6. Modulatory effects of FUS intensities on tactile network organization.** Plots of peak BOLD signal changes at FUS target and seven selected off-target ROIs during high-FUS (A), med-FUS (B), and low-FUS (C) stimulation in both resting (dotted lines) and tactile activation (solid lines) states.

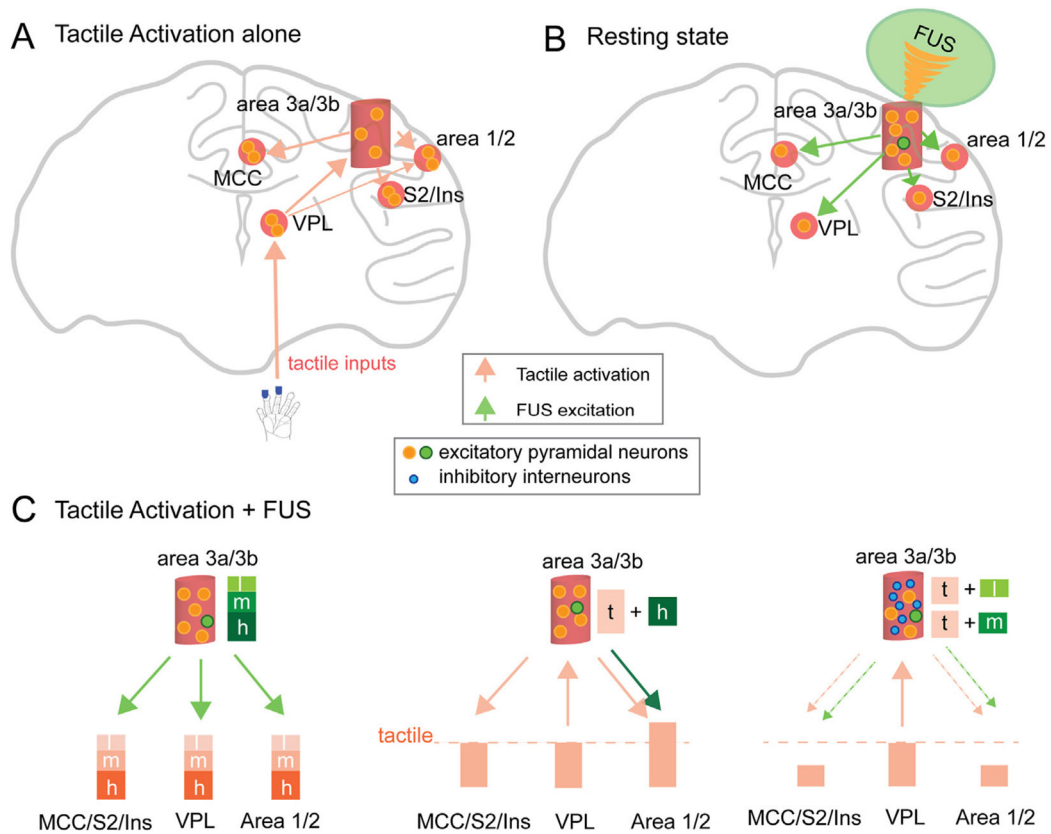


**Fig. 7. Schematic model of neuron type selective modulation of 250 kHz FUS.**

FUS modulation of two types of neurons is proposed: excitatory pyramidal neurons (large orange and green dots) and inhibitory interneurons (small blue dots). (A) Tactile stimulation of digits elicited peripheral neuron activation that projected to the thalamic VPL nucleus, then to area 3a/3b, area 1/2, and then to MCC and S2/insula. Light orange arrows indicate the direction of information flow between regions. (B) FUS directly activates area 3a/3b neurons and then the activation propagates to off-target regions. (C) Illustrations showing the net outcomes of neural signal changes at three groups of off-target regions: area 1/2, MCC/S2/insula, and VPL, and their connections to area 3a/3b. Arrows indicate the directions of activation propagation. Line thickness indicates the general strength of information flow. The dotted line indicates the magnitude of tactile stimulation evoked activation. Each of the three brain region groups represents different degrees and patterns of feedforward and feedback connections (indicated by colored arrows and directions). (Left) Three intensities of FUS-evoked graded neural activity at the targeted area 3a/3b and off-target regions at resting state. (Middle) In the high-FUS + tactile stimulation condition, high-FUS may predominantly activate a larger proportion of excitatory neurons at area 3a/3b evidenced by the lack of inhibition at this target area. Therefore, tactile responses remained unchanged in all regions except for an enhanced response in area 1/2, which receives extensive feedforward connections from area 3a/3b. (Right) Medium- and low-intensity FUS likely activated more inhibitory than excitatory neurons, therefore reducing the output signals from area 3a/3b (middle). Areas that receive inputs from area 3a/3b via feedforward connections (area 1/2, MCC, S2, and Insula) all exhibited reduced tactile signals. Tactile-

evoked neural activation signals at VPL were not affected because it is a signal feeding region to area 3a/3b via thalamocortical afferents. Signal reductions in area 3a/3b has little effect on VPL.

Author Manuscript

Author Manuscript

Author Manuscript

Author Manuscript